

Outflows from active galactic nuclei: The BLR-NLR metallicity correlation

Pu Du^{1*}, Jian-Min Wang^{1,2}, Chen Hu¹, David Valls-Gabaud^{3,1,2}, Jack A. Baldwin⁴, Jun-Qiang Ge² and Sui-Jian Xue²

¹ Key Laboratory for Particle Astrophysics, Institute of High Energy Physics, Chinese Academy of Sciences, 19B Yuquan Road, Beijing 100049, China.

² National Astronomical Observatories of China, Chinese Academy of Sciences, 20A Datun Road, Beijing 100020, China.

³ LERMA, CNRS UMR 8112, Observatoire de Paris, 61 Avenue de l'Observatoire, 75014 Paris, France.

⁴ Physics and Astronomy Department, 3270 Biomedical Physical Science Building, Michigan State University, East Lansing, MI 48824, USA.

Accepted ... Received ... ; in original form ...

ABSTRACT

The metallicity of active galactic nuclei (AGNs), which can be measured by emission line ratios in their broad and narrow line regions (BLRs and NLRs), provides invaluable information about the physical connection between the different components of AGNs. From the archival databases of the *International Ultraviolet Explorer*, the *Hubble Space Telescope* and the *Sloan Digital Sky Survey*, we have assembled the largest sample available of AGNs which have adequate spectra in both the optical and ultraviolet bands to measure the narrow line ratio $[N\ II]/H\alpha$ and also, in the same objects, the broad-line $N\ V/C\ IV$ ratio. These permit the measurement of the metallicities in the NLRs and BLRs in the same objects. We find that neither the BLR nor the NLR metallicity correlate with black hole masses or Eddington ratios, but there is a strong correlation between NLR and BLR metallicities. This metallicity correlation implies that outflows from BLRs carry metal-rich gas to NLRs at characteristic radial distances of ~ 1.0 kiloparsec. This chemical connection provides evidence for a kinetic feedback of the outflows to their hosts. Metals transported into the NLR enhance the cooling of the ISM in this region, leading to local star formation after the AGNs turn to narrow line LINERs. This post-AGN star formation is predicted to be observable as an excess continuum emission from the host galaxies in the near infrared and ultraviolet, which needs to be further explored.

Key words: galaxies: nuclei – black hole physics – galaxies: active – galaxies: abundances – accretion – ISM: outflows

1 INTRODUCTION

Accreting supermassive black holes (SMBHs) are responsible for the major phenomena observed in AGNs (e.g., see the recent review by Ho 2008), but also strongly influence their host galaxies through kinetic/radiative feedback processes (Di Matteo et al. 2005; Bower et al. 2006; Croton et al. 2006), leading to a co-evolution between the SMBHs and their hosts (e.g. Magorrian et al. 1998; Richstone et al. 1998). Many details of the specific feedback mechanisms remain under debate, but outflows have been recognised to play a key role in this co-evolution. Outflows transport energy and gas outwards from the central regions, and also carry metals to regions of galactic scales. The metallicity of the gas in AGNs can be measured in both their broad and narrow line regions, and might trace the physical relation between BLRs and NLRs. This would provide a new window for exploring the details of the feedback process.

The metallicity in broad line regions (BLRs) of AGNs has been extensively studied following the seminal paper of Hamann & Ferland (1992). Several line ratios have been suggested to measure the BLR metallicity, with the $N\ V/C\ IV$ intensity ratio being the most widely used. Many studies have confirmed the following two basic properties of the BLR metallicity: (1) it is very large, reaching as much as 10 or more times the solar abundance (Hamann & Ferland 1992, 1993; Hamann et al. 2002; Dhanda et al. 2007); and (2) it has no cosmological evolution up to redshifts $z = 6.5 \sim 7.0$ (e.g. Jiang et al. 2008; Juarez et al. 2009; Mortlock et al. 2012). There are additional –sometimes conflicting– results suggesting that metallicity correlates with either luminosity (Hamann & Ferland 1999; Dietrich et al. 2002), black hole masses (Warner, Hamann & Dietrich 2004; Matsuoka et al. 2011a,b) or Eddington ratios (Shemmer & Netzer 2002; Shemmer et al. 2004) for different samples. These properties hint at a possible production of metals in the nuclear regions and is only a local event since its timescale is much shorter than the local Hubble time. In this pic-

* E-mail: dupu@ihep.ac.cn

ture, black holes clean up the surrounding metals before the next episode of activity. This probably is linked with accretion flows, in which self-gravity drives star formation (Collin & Zahn 1999; Wang et al. 2010, 2011, 2012).

It is far more difficult to use the N v/C iv or similar ratios of UV lines to measure the metallicity in NLRs in type I AGNs, because the narrow components of lines such as N v are very faint (Nagao et al. 2006a). Only about a dozen high-redshift radio galaxies and type 2 AGNs have been measured for metallicity in this way (Nagao et al. 2006a; Matsuoka et al. 2009), for which the NLR metallicity was found to lie in the range $0.2Z_{\odot} \lesssim Z \lesssim 5.0Z_{\odot}$ with no cosmic evolution between redshifts $1.2 \leq z \leq 3.8$. This is interesting since it shows that the NLR metallicity has properties similar to those of the BLRs. The NLRs have a size¹ $R_{\text{NLR}} = 2.1 L_{[\text{O III}]\lambda 5007}^{0.5} \text{ kpc}$, where $L_{[\text{O III}]\lambda 5007} = L_{[\text{O III}]\lambda 5007}/10^{42} \text{ erg s}^{-1}$ is the [O III] $\lambda 5007$ luminosity (e.g. Bennert et al. 2002; Schmitt et al. 2003; Netzer et al. 2004). This is the typical size of a bulge. It is thus expected that the chemical properties of bulge gas can be deduced from the NLRs. However, in these type 2 objects there are no broad N v or C iv lines to measure the BLR metallicity. Obviously what is needed are measurements of both the BLR and NLR metallicities in the *same* objects, meaning in type I AGNs. This has never been done thus far.

In the interpretation of the classical Baldwin-Phillips-Terlevich (BPT Baldwin, Phillips & Terlevich 1981) diagnostic diagram, it has been suggested that the [N II]/H α line ratio acts as an indicator of the metallicity of NLRs while the [O III]/H β ratio mainly depends on the ionization parameter (see Fig. 2 in Groves, Heckman & Kauffmann 2006; Storchi-Bergmann & Pastoriza 1989; Storchi-Bergmann 1991; Storchi-Bergmann et al. 1998; Groves, Dopita & Sutherland 2004; Stasińska 2006; Nagao et al. 2006b; Kewley et al. 2013). This allows us to measure the NLR metallicity for a given ionisation parameter in type 1 AGNs and quantitatively compare it with the metallicities of the host galaxy and also of the BLR. This line ratio also provides an opportunity to *simultaneously* measure both BLR and NLR metallicities of type 1 AGNs in the same object.

In this paper we assemble from published work and data archives a sample of AGNs with spectroscopy covering a wide wavelength range that includes N v $\lambda 1240$, C iv $\lambda 1550$, [N II] $\lambda 6584$, H β and H α . This sample consists of 31 type 1 AGNs, which allow us to simultaneously measure the BLR and NLR metallicities, our goal being to test the possible connection between BLRs and NLRs. In §2 we describe the sample of AGNs, and our measurements of the BLR and NLR metallicities from both optical and UV spectra. In §3 we test for possible correlations between the NLR and BLR metallicities and of these metallicities with either black hole masses or Eddington ratios. The reliability and implications of the correlations found are discussed in §4. The cosmological parameters $H_0 = 70 \text{ km s}^{-1} \text{ Mpc}^{-1}$, $\Omega_m = 0.3$ and $\Omega_{\Lambda} = 0.7$ are assumed in this paper.

¹ Note that, in our context, the NLR does not refer to the extended narrow line regions (ENLRs), which are measured by Greene et al. (2011). The NLR size scaling law does not apply to ENLRs. Fu & Stockton (2007) find that ENLRs only appear in objects with BLR metallicities smaller than $\sim 0.6Z_{\odot}$. The typical size of NLRs of the present sample is 0.7–1.0 kpc given their [O III] luminosity of $\sim 10^{41} \text{ erg s}^{-1}$, and correspond to the bulge regions (Simard et al. 2011). The NLR and the bulge share the same approximate size.

2 THE SAMPLE OF AGNS WITH MEASURED METALLICITIES

2.1 Metallicity indicators

Our aim is to compare the BLR and NLR metallicities on an object by object basis. We use the N v/C iv ratio as a surrogate for the BLR metallicity following the well-established techniques developed by Hamann & Ferland (1992, 1993, 1999), who showed the ratio is only sensitive to metallicity rather than temperature, ionization parameter and gas density. Secondary production of N out of C and O via CNO burning dominates at metallicities $Z \gtrsim 0.2Z_{\odot}$, which result in abundance of $N \propto Z^2$, making N v/C iv flux ratio can be used as a metallicity indicator (Hamann & Ferland 1992, 1993, 1999; Hamann et al. 2002). We do not use the Fe II/H β ratio as suggested by Netzer & Trakhtenbrot (2007) since its possible correlation with BLR metallicity is a secondary result based on comparing the correlation of different line ratios with the Eddington ratio. The Fe II excitation mechanism is poorly understood and Verner et al. (2004) found that the Fe II strength is not sensitive to metallicity.

Metallicity in NLR can be indicated by the ratio of [N II]/H α as shown by Groves et al. (2006). In such a case, the ratio of narrow component N v/C iv is very tough to separate them from the spectra. The ratio of [N II]/H α is sensitive to metallicity when [N II]/H $\alpha > 0.1$ while [O III]/H β is mostly sensitive to the ionization parameter (Groves et al. 2006).

The considerations above indicate that we need a sample of objects for which there are useful measurements of at least the N v $\lambda 1240$, C iv $\lambda 1550$, H β , [O III] $\lambda 5007$, H α , and [N II] $\lambda 6584$ lines.

2.2 The samples of AGNs and quasars

We have assembled a sample which includes all of the AGNs and quasars that we know of for which it has been possible to measure both the broad N v and C iv emission lines at ultraviolet wavelengths and the narrow H β , [O III] $\lambda 5007$, H α , and [N II] $\lambda 6584$ emission lines at optical wavelengths. While there are about 900 AGNs in the *IUE* (International Ultraviolet Explorer) and *HST* (Hubble Space Telescope) data archives, only about 200 of these have also optical spectroscopy from the SDSS archive and published work. Of this subset we select only Seyfert 1 galaxies and type 1 quasars, since otherwise the N v and C iv lines are obscured by dusty tori along the line of sight. We use either *HST* spectra directly or stack all available *IUE* SWP images to produce a single co-added *IUE* spectrum. Where possible we use *HST* rather than *IUE* spectra to measure the N v/C iv ratios. We exclude objects with low signal-to-noise ratios in their stacked UV spectra, broad absorption line quasars and objects with strong C iv and N v absorption. We also exclude objects having broad Balmer emission lines which are so strong that narrow emission lines (i.e. [N II] $\lambda 6584$ and/or the narrow components of H α and H β) cannot be measured, such as bright quasars with “disappearing” narrow line regions (Netzer et al. 2004). The final sample contains 31 objects for which we can measure both the BLR metallicity and the NLR line ratios. Table 1 provides the details of the observations used in the sample.

Table 1. Optical and UV spectra of the AGN sample.

Object	Sources and references for the spectra		z	$\log L_{5100}$ (erg s^{-1})	R_{BLR} (light-day)
	Optical	Ultraviolet			
(1)	(2)	(3)	(4)	(5)	(6)
2E 1615+0611	SDSS	IUE (SWP39443, 44105, 55613)	0.038	43.25	20.2
Fairall 9*	ESO 1.5m (1)	HST/FOS (2)	0.047	44.25	16.3 [†]
HB89 1028+313	SDSS	IUE (SWP28214)	0.178	44.45	58.8
Mrk 42	SDSS	IUE (4 spectra stacked)	0.025	42.88	9.0
Mrk 106	SDSS	IUE (SWP26911)	0.123	44.52	64.0
Mrk 110	SDSS	IUE (SWP33002)	0.035	43.02	18.8 [†]
Mrk 142	SDSS	IUE (SWP20113, 20121)	0.045	43.61	21.6
Mrk 290	SDSS	IUE (5 spectra stacked)	0.030	43.60	21.3
Mrk 359	ESO 1.5m (3)	IUE (4 spectra stacked)	0.017	43.20	13.3
Mrk 493	OHP 1.93m (4)	HST/FOS (5)	0.031	43.27	14.4
Mrk 618*	WHT 4.2m (6)	IUE (SWP40871)	0.035	43.60	21.3
Mrk 771*	SDSS	IUE (SWP16880, 16884, 20142)	0.063	43.92	50.0 [†]
Mrk 841	McD 2.1m (7)	IUE (17 stacked spectra)	0.036	43.84	28.0
Mrk 876	CA 2.2/3.5m (8)	IUE (11 stacked spectra)	0.129	45.00	39.0 [†]
Mrk 1018*	SDSS	IUE (6 stacked spectra)	0.042	43.85	28.7
Mrk 1126	ESO 1.5m (3)	IUE (SWP36653, 36659)	0.011	42.71	7.4
Mrk 1239	OHP 1.93m (4)	IUE (6 stacked spectra)	0.020	43.30	14.9
Mrk 1243	SDSS	IUE (SWP36410)	0.035	43.37	16.1
Mrk 1514	WHT 4.2m (6)	HST/FOS (5)	0.016	43.41	4.9 [†]
NGC 3783*	ESO 1.5m (9)	HST/FOS (2)	0.010	43.12	4.5 [†]
NGC 4051	Bok 2.3m (10)	IUE (31 stacked spectra)	0.002	41.78 [†]	6.5 [†]
NGC 4593	WHT 4.2m (11)	IUE (29 stacked spectra)	0.009	42.75 [§]	1.2 ^{††}
NGC 5548	SDSS	HST/FOS (2)	0.017	43.31 ^{§§}	21.2 [†]
NGC 5940*	SDSS	IUE (SWP20821, 20832)	0.034	43.36	15.8
PG 0906+484*	SDSS	IUE (SWP21921, 32463)	0.117	44.10	38.7
PG 0923+129	SDSS	IUE (SWP25826)	0.029	43.39	16.5
PG 1049-005	SDSS	HST/FOS (2)	0.360	45.58	227.6
PG 1202+281	SDSS	HST/FOS (2)	0.165	44.21	44.3
SBS 1150+497	SDSS	HST/FOS (5)	0.334	44.71	80.1
Ton 256	SDSS	IUE (SWP10071)	0.131	44.52	64.2
US 1329	SDSS	IUE (SWP56263)	0.254	45.29	161.1

Columns (1), (2) and (3) list the AGN name and the source of spectral data in the optical and UV bands, respectively; columns (4), (5) and (6) give the redshift, the continuum luminosity at 5100 Å and the BLR size. For most objects, L_{5100} is measured from the optical spectra, except the following ones, for which it was taken from these references: [†] direct reverberation mapping by Kaspi et al. (2000), ^{††} from Peterson et al. (2004), [§] from Smith et al. (2004), and ^{§§} from Bentz et al. (2009). * are the sources whose broad H α and H β components have different shapes. References: (Columns 2 and 3): (1) Santos-Lleó et al. (1997); (2) Kuraszekiewicz et al. (2002); (3) Giannuzzo & Stirpe (1996); (4) Véron-Cetty, Véron & Gonçalves (2001); (5) Kuraszekiewicz et al. (2004); (6) Mullaney & Ward (2008); (7) Grupe et al. (2004); (8) Kollatschny, Zetzl & Dietrich (2006); (9) Stirpe et al. (1994); (10) Moustakas & Kennicutt (2006); (11) Dietrich et al. (1994). Spectral resolutions: IUE: $\lambda/\Delta\lambda \sim 250$; HST: $\lambda/\Delta\lambda \sim 1300$ in UV bands; SDSS: $\lambda/\Delta\lambda \sim 1800$; while the other instruments of telescopes listed in the table have $\lambda/\Delta\lambda \gtrsim 2000$.

2.3 Spectral fitting

Table 2 gives the measures of line ratios, H β FWHM, black hole masses and bolometric luminosities of the selected AGNs. Following Hu et al. (2008), we first correct the spectrum for Galactic extinction, shift it to the galaxy’s rest-frame, and fit a continuum model. The continuum model has three components: (1) a single power law; (2) Balmer continuum emission; and (3) a pseudo-continuum due to blended Fe emission.

Since the key point here is to get matched profile flux ratios to make sure that the emission lines whose fluxes are compared come from the same region, we adopt the following procedure to measure the emission lines after subtracting the continuum. In the UV spectra we model the broad-emission lines of Ly α , N v and C iv through two sets of Gaussian components each which are forced to have the same FWHM and velocity shifts. The sum of the two

Gaussian components of each line is used to obtain fluxes of the line. ² In the optical band, we fit the emission lines with three components, the same component of each line forced to have the same profile: (1) a narrow component modeled with one Gaussian each for H α , H β , [O III] $\lambda\lambda 4959, 5007$, [N II] $\lambda\lambda 6548, 6584$, [S II] $\lambda\lambda 6717, 6731$; (2) a broad component modeled with two Gaussians

² The FWHM of the narrow component of NGC 5548’s N v and C iv emission lines is 1118 km/s, which is the narrowest one in the present sample, and is marginally consistent with the criteria of broad emission line (>1000 km/s). But there is still possibility that it comes from NLR, so we relaxed the constraint of tying the profiles of the two Gaussians used to fit N v and C iv, and only use the broader components to calculate NV/CIV ratio. In this case, $\log(\text{N v}/\text{C iv})$ of NGC 5548 becomes -0.80 ± 0.04 . This number is still very similar to the value we used in the text, and does not change the conclusion at all.

Table 2. Measured and inferred quantities.

Object	$\log\left(\frac{[\text{N II}]}{\text{H}\alpha}\right)$	$\log\left(\frac{[\text{O III}]}{\text{H}\beta}\right)$	$\log\left(\frac{\text{N V}}{\text{C IV}}\right)$	FWHM	$\log M_{\bullet}$	$\log L_{\text{Bol}}$
(1)	(2)	(3)	(4)	(km s^{-1})	(M_{\odot})	(erg s^{-1})
(1)	(2)	(3)	(4)	(5)	(6)	(7)
2E 1615+0611	-0.44 ± 0.01	0.97 ± 0.01	-1.00 ± 0.07	3178	7.59	44.22
Fairall 9*	-0.17 ± 0.07	0.95 ± 0.04	-0.49 ± 0.01	5858	8.17	45.12
HB89 1028+313	-0.35 ± 0.03	1.04 ± 0.02	-0.57 ± 0.13	5794	8.73	45.31
Mrk 42	-0.35 ± 0.01	0.10 ± 0.02	-0.73 ± 0.09	973	6.37	43.90
Mrk 106	-0.40 ± 0.02	0.95 ± 0.03	-0.82 ± 0.28	4108	8.47	45.38
Mrk 110	-0.79 ± 0.02	1.01 ± 0.01	-1.08 ± 0.12	2356	7.02	44.02
Mrk 142	-0.47 ± 0.03	0.48 ± 0.13	-0.48 ± 0.10	1773	7.27	44.54
Mrk 290	-0.45 ± 0.03	1.01 ± 0.03	-0.64 ± 0.03	4000	7.97	44.53
Mrk 359	-0.41 ± 0.01	0.62 ± 0.02	-0.89 ± 0.03	887	6.46	44.18
Mrk 493	-0.29 ± 0.01	0.12 ± 0.01	-0.37 ± 0.01	886	6.49	44.24
Mrk 618*	0.02 ± 0.01	0.72 ± 0.03	-0.32 ± 0.05	2356	7.51	44.53
Mrk 771*	0.13 ± 0.05	1.14 ± 0.04	-0.36 ± 0.02	3048	8.15	44.82
Mrk 841	-0.39 ± 0.03	1.10 ± 0.03	-0.90 ± 0.33	4085	8.11	44.75
Mrk 876	-0.16 ± 0.04	0.64 ± 0.08	-0.74 ± 0.08	7781	8.65	45.83
Mrk 1018*	0.22 ± 0.06	0.77 ± 0.07	-0.22 ± 0.20	4366	8.18	44.76
Mrk 1126	0.09 ± 0.01	0.98 ± 0.02	-0.57 ± 0.19	4882	7.68	43.75
Mrk 1239	-0.30 ± 0.01	0.83 ± 0.01	-0.45 ± 0.24	951	6.57	44.26
Mrk 1243	-0.45 ± 0.05	0.58 ± 0.05	-0.26 ± 0.04	1967	7.23	44.32
Mrk 1514	-0.17 ± 0.01	0.43 ± 0.01	-0.76 ± 0.01	1967	7.08	44.36
NGC 3783*	-0.08 ± 0.03	1.00 ± 0.05	-0.65 ± 0.01	2594	7.24	44.10
NGC 4051	-0.57 ± 0.03	0.43 ± 0.06	-0.57 ± 0.03	1794	6.38	42.95
NGC 4593	0.07 ± 0.01	1.06 ± 0.03	-0.45 ± 0.06	3826	6.67	43.78
NGC 5548	-0.26 ± 0.01	1.02 ± 0.01	-0.97 ± 0.02	6378	8.36	44.28
NGC 5940*	-0.11 ± 0.03	0.89 ± 0.04	-0.46 ± 0.05	3805	7.80	44.31
PG 0906+484*	-0.25 ± 0.06	0.98 ± 0.08	-0.46 ± 0.12	4691	8.37	44.99
PG 0923+129	-0.32 ± 0.02	0.95 ± 0.02	-0.61 ± 0.05	2140	7.32	44.34
PG 1049-005	-0.53 ± 0.03	1.03 ± 0.02	-0.90 ± 0.05	5513	9.28	46.38
PG 1202+281	-0.53 ± 0.02	0.84 ± 0.01	-0.76 ± 0.01	4540	8.40	45.09
SBS 1150+497	0.05 ± 0.04	1.23 ± 0.06	-0.77 ± 0.05	4064	8.56	45.55
Ton 256	-0.51 ± 0.02	1.04 ± 0.01	-0.81 ± 0.08	2789	8.14	45.38
US 1329	-0.98 ± 0.06	0.92 ± 0.02	-0.98 ± 0.19	3827	8.81	46.10

Col. (1): object; (2): [N II] $\lambda 6584/\text{H}\alpha$ flux ratio; (3): [O III] $\lambda 5007/\text{H}\beta$ flux ratio; (4): N V $\lambda 1240/\text{C IV } \lambda 1550$ flux ratio; (5): FWHM of H β ; (6): SMBH mass; (7): bolometric luminosity. * are sources whose broad H α and H β components have different shapes.

each for H α and H β ; and (3) a wing component modeled with one Gaussian for [O III] $\lambda\lambda 4959, 5007$ when necessary. Among these lines, the flux ratios of [O III] $\lambda\lambda 4959, 5007$, [N II] $\lambda 6584$ and [N II] $\lambda 6548$ are fixed to the theoretical values of 3.0 and 2.96 respectively. There are seven sources (listed in Tables 1 and 2) showing different shapes of the broad H α and H β components. We thus relax the constraint of the FWHM and velocity shift of the corresponding Gaussians and add a third Gaussian component to them. It does not significantly affect the correlations among the line ratios and other quantities (M_{\bullet} , $L_{\text{Bol}}/L_{\text{Edd}}$). We measure the ratios [O III]/H β and [N II]/H α in the narrow components (not including the wing component of [O III]), and FWHM of broad component of H β from the fitted Gaussians which are used to model it. The continuum-subtracted spectra are provided in the Appendix as well as the corresponding results of emission-line fittings. The Appendix is provided on-line.

2.4 Estimates of SMBH parameters

To estimate the masses of the super-massive black holes (SMBHs) in our UV/optical sample, we use the empirical $R_{\text{BLR}} - L$ relation, except in objects for which direct measures from reverbera-

tion mapping observations are available. Using the host-galaxy corrected relation $R_{\text{BLR}} = 34.4 L_{44}^{0.52}$ light days (Bentz et al. 2009), where $L_{44} = L_{5100}/10^{44} \text{ erg s}^{-1}$ and L_{5100} is the continuum luminosity at 5100 Å, we have the SMBH mass from $M_{\bullet} = (f/G)R_{\text{BLR}}V_{\text{H}\beta}^2$, where G is the gravitational constant, $V_{\text{H}\beta}$ is the full-width-half maximum of the H β emission line and f is a factor determined by the geometry of the BLR. We adopt $f = 1.4$, following the calibration of the relation linking the velocity dispersion to the SMBH mass (Onken et al. 2004). We obtain the bolometric luminosity using an AGN continuum template (Marconi et al. 2004), and then the Eddington ratio from $\mathcal{E} = L_{\text{Bol}}/L_{\text{Edd}}$, where $L_{\text{Edd}} = 1.3 \times 10^{38} m_{\bullet} \text{ erg s}^{-1}$ is the Eddington limit luminosity, L_{Bol} is the bolometric luminosity and $m_{\bullet} = M_{\bullet}/M_{\odot}$.

Note that the average contributions from host galaxies (Bentz et al. 2009) is about 1/2 of the total 5100 Å luminosity. As R_{BLR} scales with the square root of the luminosity, the contaminations lead to a further uncertainty of 0.15 dex to the estimations of black hole masses as well as to the Eddington ratios. We include them in their error budget. To be conservative, we set the error bars of black hole masses, Eddington ratios and bolometric luminosity to 0.3 dex, as they are mainly determined by the systematic uncer-

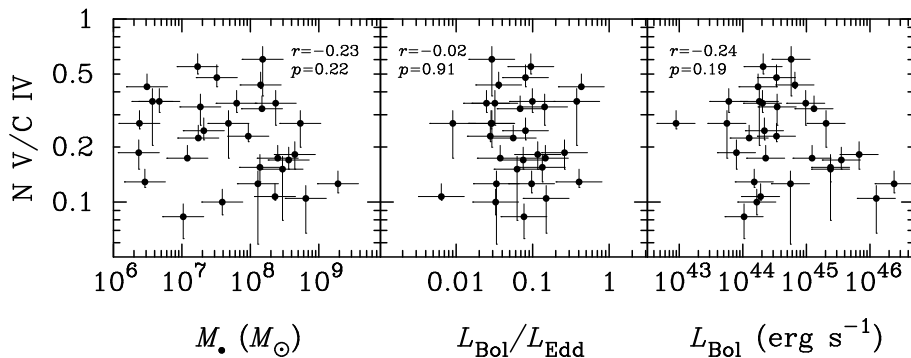


Figure 1. The line ratio of N V/C IV (BLR metallicity) versus black hole masses, Eddington ratios and bolometric luminosity. The sample shows no significant correlation between the metallicity and these parameters. Pearson’s coefficient (r) and null probability (p) are given in each panels. The BLR metallicity does not correlate with M_{\bullet} , $L_{\text{Bol}}/L_{\text{Edd}}$ or L_{Bol} .

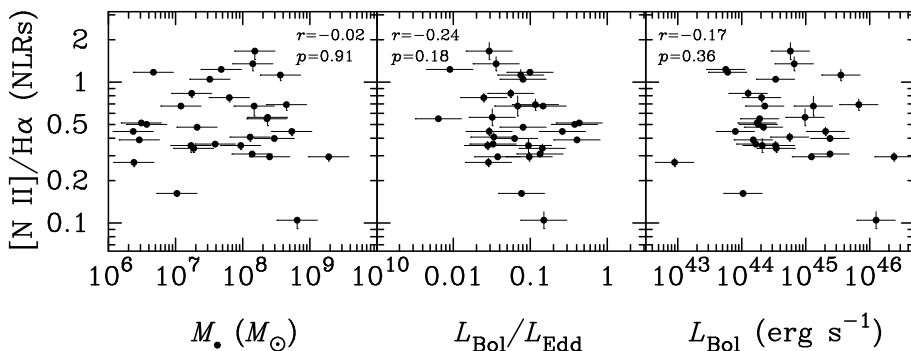


Figure 2. The line ratio of [N II]/H α (NLR metallicity) versus black hole masses, Eddington ratios and bolometric luminosity. The sample shows no correlation between the metallicity and these parameters. The error bars of black hole masses and Eddington ratios are same as in Figure 1. Pearson’s coefficient and null probability are indicated in each panel. The NLR metallicity does not correlate with any of these parameters.

tainties of f_{BLR} in the $R_{\text{BLR}} - L$ relation and host contaminations (Onken et al. 2004; Park et al. 2012; Woo et al. 2010, 2013).

3 ANALYSIS OF CORRELATIONS

3.1 BLR metallicities

Figure 1 shows that, in our carefully-selected sample, the BLR metallicities do *not* correlate with either black hole masses or Eddington ratios, or bolometric luminosity. This result can be quantitatively established through the Pearson linear correlation coefficient (r) and associated probability (p) that $|r|$ be larger than the observed value if the null hypothesis of zero correlation is true. As indicated in Figure 1, the large p values imply that the null hypothesis that the variables are not correlated is accepted in all the cases shown. Previous studies appear to give different results as listed in Table 3 for a brief summary. Warner, Hamann & Dietrich (2003) compiled a list of 578 quasars (more than 800 spectra) with redshifts $0 < z < 5$ to explore the potential relation of BLR metallicity with black hole masses and Eddington ratios. They estimated black hole masses through C IV profiles for high- z quasars, and then produced a series of composite spectra binned by black hole mass. Their sample spans 5 orders of magnitude in black hole masses and 6 orders in luminosity, and they found a correlation between Z_{BLR} and black hole masses from their stacked spectra. However, Shemmer et al. (2004) found from a detailed analysis of

high-quality spectra of 29 high- z quasars that there is *no* correlation between Z_{BLR} and black hole masses, but instead a weak correlation between the N V/C IV ratios and the Eddington ratios. Using stacked spectra of SDSS quasars with $2.3 < z < 3.0$, Matsuoka et al. (2011a) found no correlation between metallicity and Eddington ratios, but that one does exist between Z_{BLR} and black hole masses. Very recently, Shin et al. (2013) studied the metallicity of PG quasars observed by *IUE* and *HST* and found that their metallicity does not correlate with black hole masses, and perhaps weakly with Eddington ratios. The inconsistencies between these results might be due to selection effects or to the way in which the spectra were combined into composite spectra in some of the studies. The composite spectra employed in metallicity analysis may be misled by the uncertainties in black hole mass. In particular, the estimation of black hole masses in quasars through C IV should be improved somehow (Denney et al. 2013), leading to large uncertainties of Eddington ratios.

We find that our results are consistent with those of Shemmer et al. (2004), in spite of the fact that they found a weak correlation with Eddington ratio while we do not. This stems from the fact that Shemmer et al. (2004) included some high-redshift quasars and narrow-line Seyfert 1 galaxies, making their sample to be biased towards objects with larger Eddington ratios than ours. Except for these objects, the weak correlation between Z_{BLR} and Eddington ratios disappears. The correlation between Z_{BLR} and Eddington ratios is only moderate in the upper right panel of Fig-

ure 8 in Shin et al. (2013), and it disappears altogether when excluding objects with Eddington ratios $\leq 10^{-2}$. Our conclusion is that previous studies do not provide in fact any strong evidence for correlations of BLR metallicity with black hole masses or Eddington ratios, in agreement with our findings.

Our work doesn't show the correlation of BLR metallicity with bolometric luminosity which is common in previous works (Shemmer & Netzer 2002; Warner, Hamann & Dietrich 2004; Nagao et al. 2006b; Shin et al. 2013). The reason is that the bolometric luminosity of the present sample has a much smaller range than those of the previous samples ($10^{44} - 10^{45.5} \text{ erg s}^{-1}$ of L_{Bol} in the present sample, but $10^{44.5} - 10^{48.5} \text{ erg s}^{-1}$ of L_{Bol} in Warner, Hamann & Dietrich (2004), $10^{10} - 10^{14} \text{ erg s}^{-1}$ of $\nu L_{\nu}(1450\text{\AA})$ in Shemmer & Netzer (2002) and $10^{44} - 10^{46.8} \text{ erg s}^{-1}$ of L_{Bol} in Shin et al. (2013)). However, narrow spans of bolometric luminosity and Eddington ratio may provide us opportunities to find correlations which are easy to be concealed by large scatters of these parameters.

There are ten objects in common with the sample of Shin et al. (2013), and we find that their measurements of N V/C IV are in excellent agreement with ours, except for Mrk 771 and PG 1049-005. In Mrk 771, Shin et al. (2013) find N V/C IV = 0.10, but the *IUE* spectrum we analysed shows a quite strong N V feature. In PG 1049-005, they find N V/C IV = 0.71 which may be possible, given the presence of strong wings in the Ly α and C IV lines. A proper check would require high quality UV spectra). These differences do not change our results.

3.2 NLR metallicities

The [N II]/H α line ratio provides a measure of the NLR metallicity. Figure 2 shows that the NLR metallicity does not correlate with either black hole masses, bolometric luminosity or Eddington ratios, as was the case for the BLR.

A typical NLR is about the same size as a bulge, and if its metallicity is mainly contributed by stellar evolution in the bulge then the two should have metallicities which are roughly similar and which would be expected to gradually increase with cosmic time. However, the NLR metallicity in high- z radio galaxies does not correlate with redshift (Nagao et al. 2006a; Matsuoka et al. 2009). This agrees with the present results that NLR metallicity neither correlates with black hole masses nor Eddington ratios.

Additionally, the Magorrian et al. (1998) relation (that black hole masses are linearly proportional to bulges of hosts) implies that if the NLR metallicity originates from stellar evolution of bulges, there should be a correlation between black hole mass and NLR metallicity due to the well-known correlation between metallicity and galaxy masses (Tremonti et al. 2004). No such correlation is seen, again suggesting that the NLR metallicity is not dominated by metal production from the host galaxies. Furthermore, it has been found that the NLR metallicity has not undergone cosmic evolution (Matsuoka et al. 2009), but there is a trend with luminosity like the BLR metallicity (Nagao et al. 2006b). However, the metallicity in star-forming galaxies has significant cosmic evolution, decreasing with redshift (e.g. Shapley et al. 2005; Erb et al. 2006). The question that arises, given that, the metallicity in NLRs maybe not produced by the host galaxy, is: what could possibly be its origin?

3.3 The BLR-NLR metallicity correlation

Figure 3 compares the NLR and BLR metallicities, and shows that they are strongly correlated given the regression coefficient $r = 0.58$ and the null probability of no correlation $p = 5.7 \times 10^{-4}$. The strong correlation is surprising because BLRs and NLRs are separated by scales of about 1.0 kiloparsec. Their metallicities indicate that these two separated regions are in fact physically connected, but *how* do they connect?

The correlation cannot be caused by ionisation parameter effects. The N V/C IV broad line ratio is weakly proportional to the ionisation parameter (Ξ_{BLR}) (see Fig. 4. in Hamann et al. 2002) whereas the [N II]/H α narrow line ratio is approximately inversely proportional to $\log \Xi_{\text{NLR}}$ (Fig. 8 in Dopita et al. (2000), Fig. 8 in Kewley & Dopita (2002) and Fig. 13 Nagao et al. (2006b)). On the other hand, Ξ_{BLR} and Ξ_{NLR} could be very different from each other. The present correlations as shown by Fig. 3 are thus not be caused by Ξ_{BLR} and Ξ_{NLR} (estimated in § 4.2) in the present sample.

The spectral energy distributions (SEDs) of the central engines may influence the line ratios of N V/C IV. As the SEDs are controlled by the Eddington ratios (Wang, Watarai & Mineshige 2004; Shemmer et al. 2006; Brightman et al. 2013), the correlation between BLR-NLR metallicity can not be caused by the different SEDs because the distribution of the Eddington ratios in the present sample is very narrow. The gas density in NLR should not exceed about 10^5 cm^{-3} , above which forbidden lines are highly suppressed. Furthermore, as indicators of metallicity in BLR and NLR, the two line ratios are not sensitive to gas density.

We are therefore led to conclude that there is a link between the metallicities in the NLR and in the BLR in these objects.

4 DISCUSSION

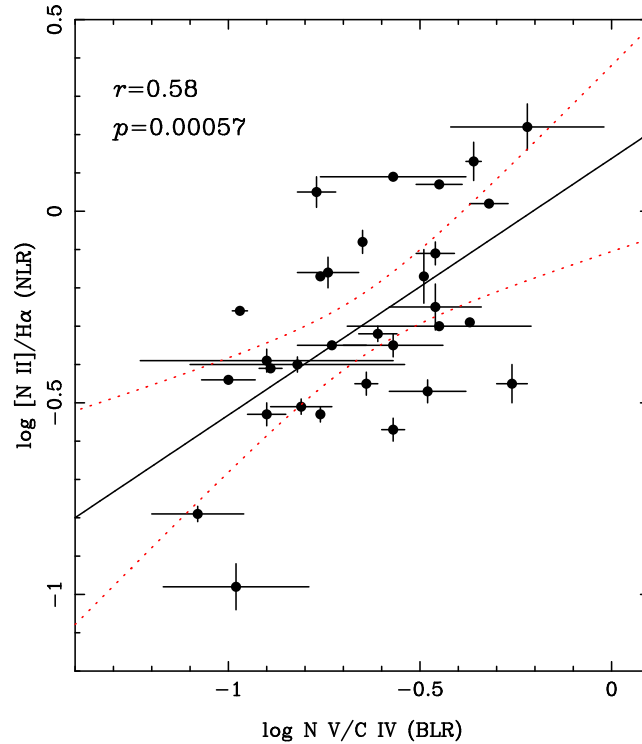
Several models exist in which BLR metals are produced by bursts of star formation in the accretion flows that are fueling the central black holes (Collin & Zahn 1999, 2008; Wang et al. 2010, 2011, 2012, e.g.), but the large metallicity in NLRs remains intriguing. The key question is to understand how the metallicity can be correlated in these two regions which have such different characteristic sizes? Even though the ionised gas in NLRs is mainly supplied by stellar winds from the bulge, the NLR metallicity of the ionised gas can be strongly affected by outflows developed from the central regions of AGNs. The metals delivered to the NLRs by the outflows, specifically by outflows from the BLRs, might enhance the metallicity in NLRs.

4.1 Metals produced in BLRs

It is generally accepted that black holes grow episodically with cosmic time (Small & Blandford 1992; Marconi et al. 2004; Wang et al. 2006, 2008). The absence of metallicity evolution on cosmological timescales (Hamann & Ferland 1999; Warner, Hamann & Dietrich 2003) strongly indicates that, for every episode, the star forming discs initially start from a larger reservoir of gas having the metallicity of the host galaxy, rather than being steadily built up as the same gas cycles through many episodes. This is consistent with the theoretical expectation for a single episode of SMBH activity (Wang et al. 2010, 2011). In this model, metals are produced in the self-gravitating part of accretion discs as a result of supporting the Shakura-Sunyaev disc

Table 3. A summary of the previous results of correlations of Z_{BLR} with central engines

References	sample	$L_{\text{Bol}}/L_{\text{Edd}}$	M_{\bullet}	L_{UV} or M_B	Notes
Hamann & Ferland (1993)	~ 100 quasars ($0 \lesssim z \lesssim 5$)	yes, but weak	both N V/C IV, He II/C IV
Shemmer & Netzer (2002)	162 AGNs (including 8 NLS1)	yes	weakened by NLS1s
Warner et al. (2003; 2004)	578 quasars ($0 \lesssim z \lesssim 5$)	No	yes	yes	composite spectra
Shemmer et al. (2004)	29 quasars ($z \approx 2 \sim 3$)+92 AGNs	...	yes	very weak	only N V/C IV
Nagao et al. (2006)	~ 5000 SDSS quasars DR2 ($2.0 \lesssim z \lesssim 4.5$)	yes	composite spectra
Matsuoka et al. (2011)	~ 2383 SDSS quasars ($2.3 \lesssim z \lesssim 3.0$)	yes	yes	yes	composite spectra, but only N V/C IV, He II/C IV
Shin et al. (2013)	70 PG quasars ($z < 0.5$)	yes, but moderate	very weak	yes, but weak	both N V/C IV, He II/C IV


Figure 3. NLR metallicities versus BLR metallicity. The correlation found in this sample is highly significant (the red dotted line mark the 95%-level confidence boundaries for the linear regression given by the black line) and is not caused by ionisation parameters (see § 3.3 for details).

(Shakura & Sunyaev 1973) around SMBHs (Wang et al. 2010). BLRs are much more metal-rich than their host galaxies, and therefore the excess metals cannot be the products of the stars in the host galaxies. In this picture, a black hole’s accretion rate stays approximately constant during a single AGN episode, but the BLR’s metallicity increases monotonically with time, and is regarded as a probe of age of the particular AGN episode. In this model, no strong correlation is expected between metallicity and either the black hole masses or Eddington ratios.

On the other hand, the peak metallicity reached during each episode (Fig. 3 *left* panel in Wang et al. (2011)) might correlate with the Eddington ratio. The individual objects within a sample of AGNs will have different ages within their respective episodes, and different samples will have different mixtures of ages, which may explain the variety of results (i.e. lack or presence of correlations between metallicities and Eddington ratios, black hole masses and luminosities) found in different studies.

4.2 Emitting clouds in NLRs

Before addressing possible mechanisms which can account for the observed correlation between the metallicities in the BLR and NLR, the issue of the role of variations in the ionisation parameter Ξ must be assessed in the robustness of the measure of metallicity through the $[\text{N II}]/\text{H}\alpha$ line ratios. Inspired by the fact that the extended NLRs are at a radial distance from the AGN that is similar to the size of the bulge (Bennert et al. 2002; Schmitt et al. 2003; Netzer et al. 2004), we explore the NLR physics within the framework of the coevolution of SMBHs and galaxies (Richstone et al. 1998) in order to understand the evolutionary tracks of AGNs. A key assumption is that the NLR clouds are pressure confined by the hot gas from stellar winds in the bulge. The main features of the NLR model are: (1) a two-phase medium composed of cold clouds and a hot medium; (2) a hot medium from stellar winds in the bulges (Ho 2009), ionised by the central engine radiation and cooled via line emission; (3) cold clouds formed from AGN outflows whose evidence comes by the usual blue shift of $[\text{O III}]$; and (4) a star forming disc that produces metals continuously, which

are then transported outwards by AGN outflows. The last two assumptions are supported by the strong correlation of NLR and BLR metallicities. Assuming photoionisation, we give a simple estimate of the properties of the NLR line emission as follows.

The ionisation parameter is defined by $\Xi_{\text{NLR}} = L_{\text{ion}}/4\pi R_{\text{NLR}}^2 c n_e k T_e$, where L_{ion} is the ionising luminosity, c and k are the speed of light and the Boltzmann constant, respectively, R_{NLR} is the NLR size, and n_e and T_e are the density and the temperature of the ionised gas of cold clouds in the NLR. Considering the relation $R_{\text{NLR}} \propto L_{[\text{OIII}]}^{1/2} \propto L_{\text{ion}}^{1/2}$, we have $\Xi_{\text{NLR}} \propto (n_e T_e)^{-1}$. We assume that the NLR is composed of numerous discrete clouds, which are confined by the surrounding hot interstellar medium (ISM) from stellar winds in bulges (Ho 2009). In such a simple two-phase model, the pressure balance equation reads $n_e T_e = n_h T_h$, where n_h and T_h are the density and temperature of the hot ISM. For the simplest consideration, the hot ISM has a virialised temperature of $k T_h \approx G M_{\text{bulge}}/R_{\text{NLR}}$. Considering the Magorrian relation $M_{\bullet} \propto M_{\text{bulge}}$ (Magorrian et al. 1998) and $R_{\text{NLR}} \propto L^{1/2} \propto (\mathcal{E} M_{\bullet})^{1/2}$, we have $T_h \propto (M_{\bullet}/\mathcal{E})^{1/2}$. It has been suggested that, in the bulge, the hot ISM is eventually accreted onto the SMBH without going through a static state (Ho 2009). For a simple version of the inflows in the bulge, the mass rate is given by $\dot{M}_{\text{inflow}} = 4\pi R_{\text{NLR}}^2 V_{\text{ff}} n_h m_p$, where $V_{\text{ff}} = (G M_{\text{bulge}}/R_{\text{NLR}})^{1/2}$ is the free-fall speed of the hot gas and M_{bulge} is the mass of the bulge. We assume a simple relation between the SMBH accretion rate (\dot{M}_{\bullet}) and the inflow, so that $\dot{M}_{\bullet} \propto \mathcal{E} \dot{M}_{\text{inflow}}$, yielding the scaling relation

$$n_h \propto \mathcal{E} R_{\text{NLR}}^{-3/2} M_{\text{bulge}}^{1/2} \propto \left(\frac{\mathcal{E}}{M_{\bullet}}\right)^{1/4}. \quad (1)$$

As the thermal pressure of the hot ISM is $n_h T_h \propto (\mathcal{E}/M_{\bullet})^{-1/4}$, we find that

$$\Xi_{\text{NLR}} \propto (n_e T_e)^{-1} \propto \left(\frac{\mathcal{E}}{M_{\bullet}}\right)^{1/4}. \quad (2)$$

This yields a range of ionisation parameter as $\Delta \log \Xi_{\text{NLR}} = 0.25 \Delta \log (\mathcal{E}/M_{\bullet})$. From Fig. 1, the scatter of the present sample is $\Delta \log \mathcal{E} \sim 2.0$ and $\Delta \log M_{\bullet} \sim 3.0$, which implies that $\Delta \log \Xi_{\text{NLR}} \sim 1.5$. In the detailed calculations of Groves, Heckman & Kauffmann (2006), the ratio of $[\text{N II}]/\text{H}\alpha$ is sensitive to the metallicity if the ionisation parameter is within a range of $\Delta \log \Xi \sim 2.5$. In the case of the highest sensitivity to the ionisation parameters, we find $[\text{N II}]/\text{H}\alpha \propto \Xi^{0.3-0.5}$ (for a fixed metallicity of $4Z_{\odot}$). The ionisation parameters of the present sample are within the range of validity of the Groves et al. models. This justifies the use of the $[\text{N II}]/\text{H}\alpha$ line ratios as a proper metallicity indicator. The recent grid of state-of-the-art models by Kewley et al. (2013) confirms these trends.

4.3 Metallicity in the NLR

Figure 4 shows the BPT diagram of the present sample. Groves, Heckman & Kauffmann (2006) found that, approximately, $Z_{\text{NLR}} \approx 1.0 + 3.0 \{ \log [\text{NII}] / \text{H}\alpha + 1 \}$ for $[\text{N II}]/\text{H}\alpha \geq 0.1$ (from their Figure 2, neglecting the dependence on ionisation parameter). We have a range of metallicity $Z_{\text{NLR}} \approx (1 - 4)Z_{\odot}$ (corresponding to $[\text{N II}]/\text{H}\alpha = 0.1-1.5$) in our sample. This is further confirmed by recent state-of-the-art models (Kewley et al. 2013) which also show that the current sample has this range of metallicities, irrespective of the SEDs and/or the ionisation parameter (see their Fig. 4, and note that the updated solar abundance is, in that scale,

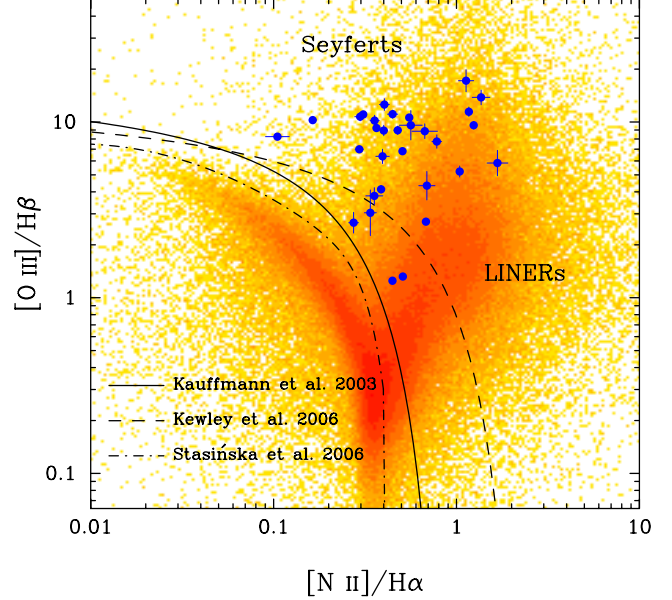


Figure 4. The Baldwin-Phillips-Terlevich diagnostic diagram of the present sample of 31 AGNs (blue filled circles). The yellow background is the sample of Seyfert 2, star-forming galaxies, HII galaxies, and LINERs from the MPA compilation of the SDSS sample (available at www.mpa-garching.mpg.de/SDSS) adopting a $S/N > 3$ limit for the four lines involved. The black solid (Kauffmann et al. 2003), dashed (Kewley et al. 2006) and dot-dashed lines (Stasińska et al. 2006) are different criteria used to separate AGNs from star-forming galaxies.

of $12 + \log(\text{O}/\text{H}) = 8.69 \pm 0.05$, Asplund et al. 2009). NLRs have metallicities ranging between the values found in the bulge and in the BLR, according to measurements made in a few objects (Matsuoka et al. 2009). These preliminary results also indicate that the metallicity in the NLR correlates with emission line luminosity rather than with redshift (Matsuoka et al. 2009).

As Fig. 3 shows, the metallicity of discrete cold clouds in the NLR follows that of the BLR, indicating an origin closely connected to the BLR. One natural way for this to happen is AGN outflows, which may causally connect the BLR and the NLR. For example, quite a large fraction of $[\text{O III}]$ lines have blue-shifted wings, indicating the importance of outflows in the NLR (Komossa et al. 2008), and more generally these outflows are linked to the feedback processes (see the detailed discussion by Nesvadba et al. 2006). Cold clouds may partially involve the hot gas from stellar winds in the bulge (Ho 2009). We represent the metallicity in the NLR by

$$Z_{\text{NLR}} = f_{\text{bulge}} Z_{\text{bulge}} + (1 - f_{\text{bulge}}) Z_{\text{BLR}}, \quad (3)$$

where $f_{\text{bulge}} = \dot{M}_{\text{bulge}}/(\dot{M}_{\text{bulge}} + \dot{M}_{\text{outflow}})$, and \dot{M}_{bulge} is the mass rate of stellar winds from stars in the bulge. The factor f_{bulge} could be significantly smaller than unity (for some redshifts) and $Z_{\text{bulge}} \ll Z_{\text{BLR}}$, leading to $Z_{\text{NLR}} \approx (1 - f_{\text{bulge}})Z_{\text{BLR}} < Z_{\text{BLR}}$, so that $Z_{\text{BLR}} \propto Z_{\text{NLR}}$ is indeed expected. The correlation found in Fig. 3 strongly supports this hypothesis.

The metallicity in the bulges, for example, of massive star forming galaxies ($10^{10-11} M_{\odot}$) is in the range $Z_{\text{SF}} \approx (2 - 3)Z_{\odot}$ (e.g. see Fig. 6 in Tremonti et al. 2004), whereas the metallicity of NLRs in typical AGNs is of $Z_{\text{NLR}} \approx (2 - 4)Z_{\odot}$ (Kewley et al. 2013). However, the comparison of Z_{bulge} with Z_{NLR} is open for the same individual objects, leading to difficulties to estimate the factor f_{bulge} . Future studies on this issue will examine several im-

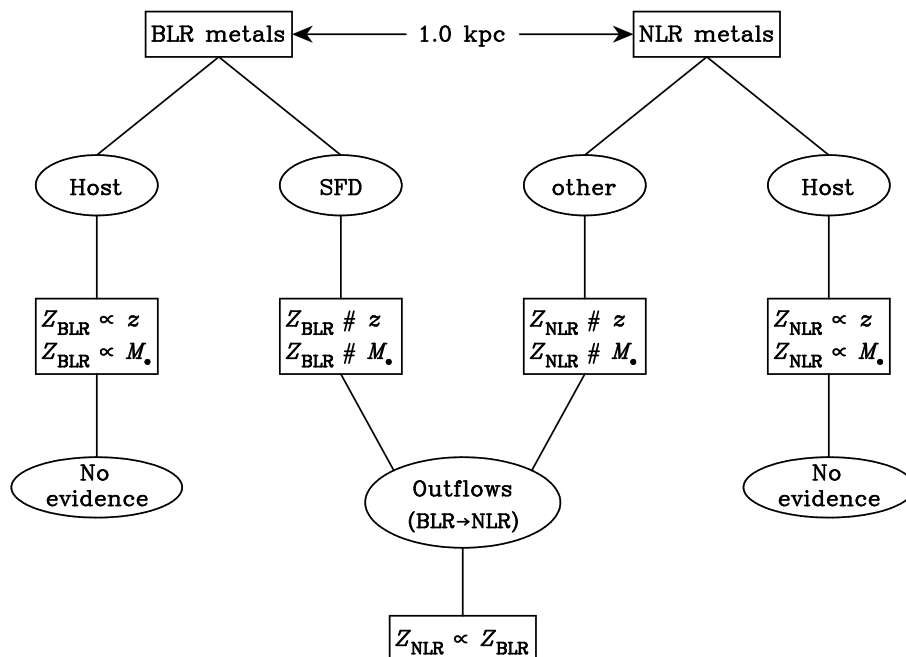


Figure 5. Flow chart of the arguments in this paper. If metals are produced by the processes shown in the ovals on the second line, correlations should follow as indicated on the third line. The results found in this work favour that BLRs and NLRs are connected through outflows developed from BLRs. “SFD” refers to “star forming disc”, which is the self-gravity-dominated regions of accretion disks (e.g. Wang et al. 2012). “Other” refers to any processes for NLR metal production except for the normal chemical evolution of the host galaxy, including star formation related to the AGN accretion process. The symbols \propto and $\#$ indicate “correlated with” and “not correlated with”, respectively.

portant physical processes (see a brief discussion at the end of this section).

A caveat may arise from the fact that while our sample clearly follows the expected distribution of Seyfert 2 galaxies with $Z_{\text{NLR}} \approx (1 - 4)Z_{\odot}$ in the BPT diagram, it perhaps does not trace the underlying density given by the SDSS sample (i.e. perhaps a larger number of blue points should lie towards the LINER area in Fig. 4). The reason for this effect is unclear, as our sample is not biased in any of the quantities involved here. It may reflect the small size of the current sample or perhaps be linked to selection effects within the framework of AGN unification schemes (e.g. Zhang et al. 2008).

The chemical abundance connection between BLRs and NLRs found here provides a new clue for understanding the structure of AGNs. As a brief summary, Fig. 5 shows a flow chart of the arguments presented in this paper. If the metals in BLRs are produced by the host galaxies, two correlations are then expected: $Z_{\text{BLR}} \propto z$ and $Z_{\text{BLR}} \propto M_*$. Neither is supported by any observational evidence. The same reasoning applies to NLRs. Hence, the only scenario that can explain the present results includes: (1) a star-forming disc which produces the metals within the BLR clouds; and (2) outflows produced in the BLR transport gas, including metals, to the NLR.

These outflows will impact the host galaxies. The kinematical effects on the host galaxy’s ISM and on the further growth of the host galaxy are discussed by Nesvadba et al. (2006). However, the BLR-NLR metallicity correlation found here is a new aspect of AGN feedback, which has additional observable consequences which we discuss next.

The metallicities of NLRs and of the host galaxies need to be compared for individual objects in the future. But we would like to

point that the $Z_{\text{BLR}} - Z_{\text{NLR}}$ correlation found in this paper indicate that Z_{NLR} should be larger than that of the host galaxy, otherwise the correlation should disappear. Observations with Integral Field Units (IFU) may explore the differences in NLR metallicities from their hosts by comparing the metallicity within the ionisation cone (i.e. the NLR) and outside of the cone. This will test the chemical evolution and circulation from the BLR and NLR to the host galaxies.

4.4 Post-AGN star formation

The metallicity correlation between BLRs and NLRs has an interesting implication for the further evolution of the AGN and its host galaxy. During the active episodic phase, metals are transported by outflows enriching the NLRs. The diffusion time scale of metals is $t_{\text{diff}} \sim R/c_s \approx 10^7 R_{1\text{kpc}} T_6^{-1/2}$ years, where $c_s \approx 10^7 T_6^{1/2} \text{cm s}^{-1}$ is the sound speed, and is much longer than the time scale for metal transportation by outflows $t_{\text{outflow}} \sim R/V_{\text{out}} \sim 3.3 \times 10^5 R_{1\text{kpc}} V_{0.01}^{-1}$ years, where $V_{0.01} = V_{\text{out}}/0.01c$ (see a brief review by Cappi et al. 2013). This means that metals remain in the NLR gas clouds once they have been transported there. The metals will significantly shorten the cooling timescale³ of the interstellar medium (ISM) in the bulge. Normally the cooling could

³ Approximated by $t_{\text{cooling}} \approx 2.3 \times 10^5 n_{\text{ISM},1}^{-1} T_6^{1+\gamma} Z_{0.1}^{-1}$ years, where $n_{\text{ISM},1} = n_{\text{ISM}}/1.0 \text{cm}^{-3}$ is the ISM density and $Z_{0.1} = Z_{\text{ISM}}/0.1Z_{\odot}$ is ISM metallicity. If $t_{\text{heating}} > t_{\text{cooling}}$, the ISM cooling is not balanced by the heating, and the ISM will condense and form stars. The dissipation time scale of the kinetic energy of outflows can be approximated by t_{outflow} , and thus $t_{\text{heating}} \approx t_{\text{cooling}}$ is expected.

be balanced by the AGN heating (radiative and kinetic of outflows) and other sources of heating. However, as a result of the metal enrichment of the ISM, t_{cooling} could be shorter than t_{heating} , leading to star formation as soon as AGNs have faded away and turned into LINERs (e.g. Wang & Zhang 2007; Ho 2008). In this case, the accretion rates of black holes become so low that no broad components of the emission lines appear in these LINERs, but significant star formation will begin after the outflows from the nuclei have been quenched. We will call these objects *blue* LINERs whereas LINERs without significant star formation will be called *red* LINERs.

Detailed calculations are needed in order to fully predict the observable signatures of this post-AGN star formation in blue LINERs, but the major features are expected to be: (1) only narrow emission lines should be seen; and (2) a population of young stars should produce significant near infrared emission and/or an ultraviolet excess from massive stars. LINERs from blue to red represent a sequence of decreasing star formation rates, and thus constitute an evolutionary sequence for the fading of AGNs. The fact that the $[\text{N II}]/\text{H}\alpha$ ratio in LINERs is larger than in star forming galaxies could imply that the emission line regions in LINERs are more metal rich than those in star forming galaxies (This should be demonstrated by both theory and observations in the future). This might be caused by post-AGN star formation further enhancing the metallicity in the LINERs. Future systematic examinations using *Spitzer* and *Herschel* observations should be able to discover these blue LINERs, providing new clues for the understanding of the physical processes of AGN fading.

5 CONCLUSIONS

We have carefully assembled in this paper a sample of AGNs and quasars with redshifts $z \lesssim 0.35$ for which the metallicity of both the BLR and the NLR can be measured in the optical and UV bands. This allows us to explore the physical connections between broad and narrow line regions and we find no correlation between metallicity and black hole masses or Eddington ratios in either BLRs or NLRs. However, we do find that the metallicities in the NLR follow the metallicities in the BLR, with both being substantially enriched above the level of the stellar populations in the bulges of the host galaxies. This suggests that metals are produced in the BLRs and then transported to the NLRs through outflows. The metal-enriched NLRs may undergo star formation once AGNs begin turning into LINERs, that is, some post-AGN star formation might be triggered. There is preliminary evidence for this process, but future surveys of post-AGN LINERs are needed to fully unveil this mechanism.

ACKNOWLEDGEMENTS

The authors acknowledge useful comments and suggestions by the anonymous referee. We also appreciate the stimulating discussions carried out with members of the AGN group at IHEP. This research is supported by grants NSFC-11173023, -11233003 and the 973 project (2009CB824800). JMW was also supported by the Sino-French LIA ORIGINS (CNRS/CAS) and by the Observatoire de Paris (poste rouge). DVG was partly supported by a visiting professorship for senior international scientists (Chinese Academy of Sciences). JAB acknowledges support from NSF grant AST-1006593.

REFERENCES

- Asplund, M. et al. 2009, *Ann. Rev. A & A*, 47, 481
 Baldwin, J. A., Phillips, M. M. & Terlevich, R. 1981, *Pub. Ast. Soc. Pacific*, 93, 5
 Bennert, N. et al. 2002, *ApJ*, 574, 105
 Bentz, M. et al. 2009, *ApJ*, 697, 160
 Brightman, M. et al. 2013, *MNRAS*, 433, 2485
 Bower, R. G. et al. 2006, *MNRAS*, 370, 645
 Cappi, M., Tombesi, F. & Giustini, M. arXiv1301.7199
 Collin, S. & Zahn, J.-P. 1999, *A&A*, 344, 433
 Collin, S. & Zahn, J.-P. 2008, *A&A*, 477, 419
 Croton, D. J. et al. 2006, *MNRAS*, 365, 11
 Denney, K.D., Pogge, R.W., Assef, R.J. et al. 2013, *ApJ*, 775, 60
 Dhandu, N., Baldwin, J. A., Bentz, M. C., & Osmer P. S. 2007, *ApJ*, 658, 804
 Dietrich, M. et al. 1994, *A&A*, 284, 33
 Dietrich, M. et al. 2002, *ApJ*, 581, 912
 Di Matteo, T., Springel, V. & Hernquist, L. 2005, *Nature*, 433, 604
 Dopita, M.A. et al. 2000, *ApJ*, 542, 224
 Erb, D. K. et al. 2006, *ApJ*, 644, 813
 Fu, H. & Stockton, A. 2007, *ApJ*, 664, L75
 Giannuzzo, M. E. & Stirpe, G. M. 1996, *A&A*, 314, 419
 Greene, J. et al. 2011, *ApJ*, 732, 9
 Groves, B. A., Dopita, M. A. & Sutherland, R. S. 2004, *ApJS*, 153, 75
 Groves, B. A., Heckman, T. M. & Kauffmann, G. 2006, *MNRAS*, 371, 1559
 Grupe, D. et al. 2004, *AJ*, 127, 156
 Hamann, F. & Ferland, G. 1992, *ApJ*, 391, L53
 Hamann, F. & Ferland, G. 1993, *ApJ*, 418, 11
 Hamann, F. & Ferland, G. 1999, *Ann. Rev. A & A*, 37, 487
 Hamann, F. et al. 2002, *ApJ*, 564, 592
 Ho, L. C. 2008, *Ann. Rev. A & A*, 46, 475
 Ho, L. C. 2009, *ApJ*, 699, 638
 Hu, C. et al. 2008, *ApJ*, 687, 78
 Juarez, Y., Maiolino, R. & Nagao, T. 2009, *A&A*, 494, L25
 Jiang, L., Fan, X. & Vestergaard, M. 2008, *ApJ*, 679, 962
 Kaspi, S. et al. 2000, *ApJ*, 533, 631
 Kauffmann, G. et al. 2003, *MNRAS*, 346, 1055
 Kewley, L. J. & Dopita, M. A. 2002, *ApJS*, 142, 35
 Kewley, L., Groves, B., Kauffmann, G. & Heckman, T. 2006, *MNRAS*, 372, 961
 Kewley, L.J., Dopita, M.A., Leitherer, C. et al. 2013, *ApJ*, 774, 100
 Kollatschny, W., Zetzl, M. & Dietrich, M. 2006, *A&A*, 454, 459
 Komossa, S., Xu, D., Zhou, H., Storchi-Bergmann, T. & Binette, L. 2008, *ApJ*, 680, 926
 Kuraszkiwicz, J. K. et al. 2002, *ApJS*, 143, 257
 Kuraszkiwicz, J. K. et al. 2004, *ApJS*, 150, 165
 Magorrian, J. et al. 1998, *AJ*, 115, 2285
 Marconi, A. et al. 2004, *MNRAS*, 351, 169
 Matsuoka, K. et al. 2009, *A&A*, 503, 721
 Matsuoka, K. et al. 2011a, *A&A*, 527, 100
 Matsuoka, K. et al. 2011b, *A&A*, 532, L10
 Mortlock, D. J. et al. 2012 *Nature*, 474, 616
 Moustakas, J. & Kennicutt, R. 2006, *ApJS*, 164, 81
 Mullaney, J. R. & Ward, M. J. 2008, *MNRAS*, 385, 53
 Nagao, T., Maiolino, R. & Marconi, A. 2006a, *A&A*, 447, 863
 Nagao, T., Maiolino, R. & Marconi, A. 2006b, *A&A*, 447, 157
 Nagao, T., Maiolino, R. & Marconi, A. 2006c, *A&A*, 459, 85
 Nesvadba, N., Lehnert, M., Eisenhauer, F. et al. 2006, *ApJ*, 650,

693

- Netzer, H. et al. 2004, ApJ, 614, 558
 Netzer H. & Trakhtenbrot, B. 2007, ApJ, 654, 754
 Onken, C. A. et al. 2004, ApJ, 615, 645
 Park, D. et al. 2012, ApJS, 203, 6
 Peterson, B. M. et al. 2004, ApJ, 613, 682
 Richstone, D. et al. 1998, Nature, 395, A14
 Santos-Lleó, M. et al. 1997, ApJS, 112, 271
 Schmitt, H. R. et al. 2003, ApJ, 597, 768
 Shakura, N. I., Sunyaev, R. A. 1973, A&A, 24, 337
 Shapley, A. E., Coil, A. L., Ma, C.-P & Bundy, K. 2005, ApJ, 635, 1006
 Simard, L. et al. 2011, ApJS, 196, 11
 Shemmer, O. & Netzer, H. 2002, ApJ, 567, L19
 Shemmer, O. et al. 2004, ApJ, 614, 547
 Shemmer, O. et al. 2006, ApJ, 646, 29
 Shin, J. et al. 2013, ApJ, 763, 58
 Smith, J. E. et al. 2004, MNRAS, 350, 140
 Small, T. A. & Blandford, R. D. 1992, MNRAS, 259, 725
 Stasińska, G. 2006, A&A, 454, L127
 Stasińska, G., Cid Fernandes, R., Mateus, A., Sodré, L., Asari, N. V. 2006, MNRAS, 371, 972
 Stirpe, G. M. et al. 1994, ApJ, 425, 609
 Storchi-Bergmann, T. & Pastoriza, M. G. 1989, ApJ, 347, 195
 Storchi-Bergmann, T. 1991, MNRAS, 249, 404
 Storchi-Bergmann, T. et al. 1998, AJ, 115, 909
 Tremonti, C. A. et al. 2004, ApJ, 613, 898
 Verner, E. et al. 2004, ApJ, 611, 780
 Véron-Cetty, M.-P., Véron, P. & Gonçalves, A. C. 2001, A&A, 372, 730
 Wang, J.-M., Watarai, K.-Y. & Mineshige, S. 2004, ApJ, 607, 107
 Wang, J.-M., Chen, Y.-M. & Zhang, F. 2006, ApJ, 647, L17
 Wang, J.-M. & Zhang, E.-P. 2007, ApJ, 660, 1072
 Wang, J.-M., Chen, Y.-M., Yan, C.-S. & Hu, C. 2008, ApJ, 673, L9
 Wang, J.-M. et al. 2010, ApJ, 719, L148
 Wang, J.-M., Ge, J.-Q., Hu, C., Baldwin, J. A., Li, Y.-R., Ferland, G., Yan, C.-S., Xiang, F. & Zhang, S. 2011, ApJ, 739, 3
 Wang, J.-M., Du, P., Baldwin, J. A., Ge, J.-Q., Hu, C. & Ferland, G. 2012, ApJ, 746, 137
 Warner, C., Hamann, F. & Dietrich, M. 2003, ApJ, 596, 72
 Warner, C., Hamann, F. & Dietrich, M. 2004, ApJ, 608, 136
 Woo, J.-H. et al. 2010, ApJ, 716, 269
 Woo, J.-H. et al. 2013, ApJ, 772, 49
 Zhang, K., Wang, T.-G., Dong, X.-B. & Lu, H.-L. 2008, ApJ, 685, L109

APPENDIX A: EMISSION LINE FITTINGS

Figure A1 presents the details of the fitted spectra for the individual objects of the present sample and is provided online. We would like to point out that they are continuum-subtracted spectra, i.e. subtracting a power-law, Fe II and Balmer continuum.

This paper has been typeset from a $\text{\TeX}/\text{\LaTeX}$ file prepared by the author.

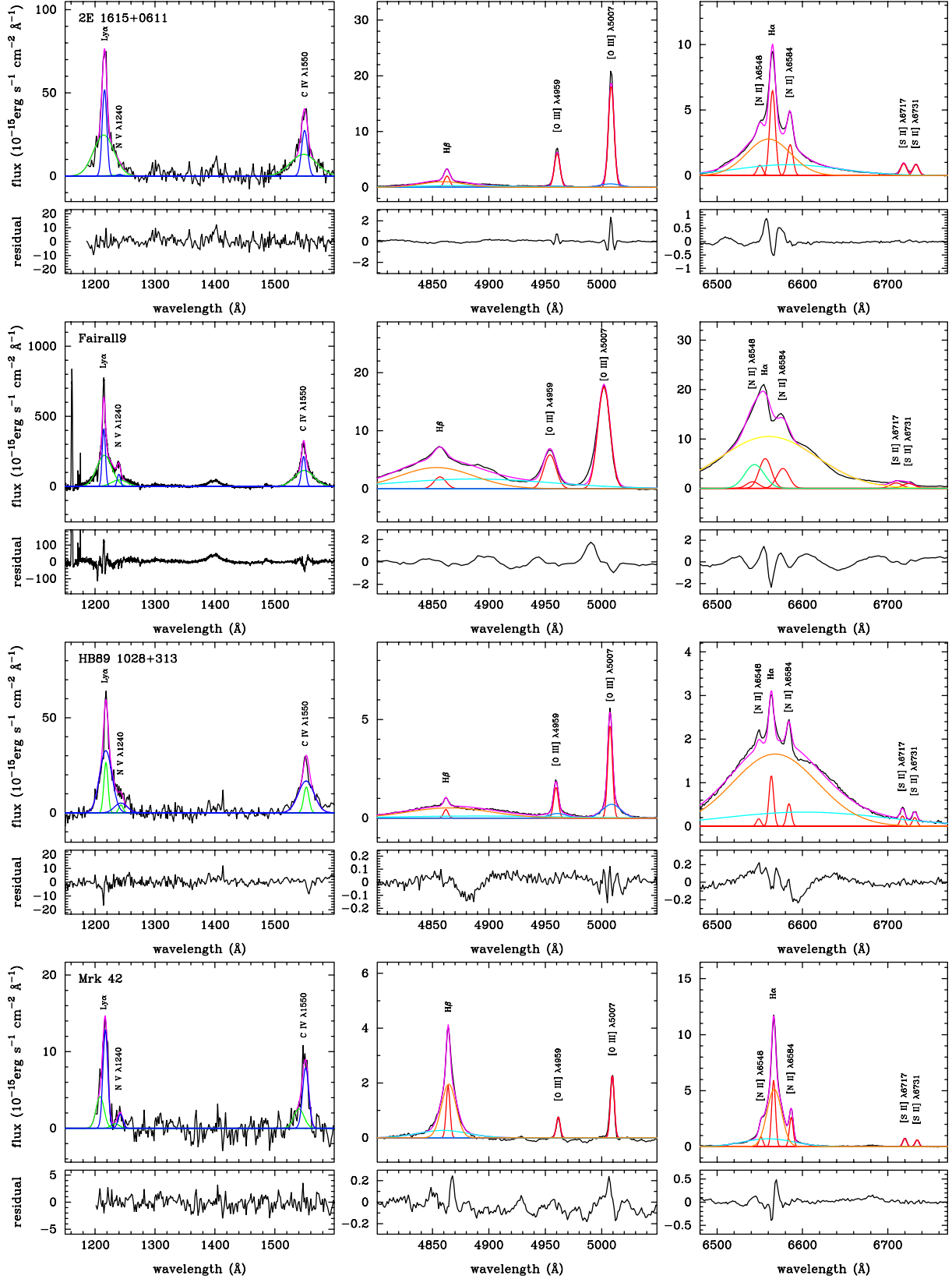


Figure A1. Continuum-subtracted spectra and results of emission-line fittings. *Left:* UV spectra for N V/C IV; *middle:* optical band for H β and [O III]; and *right:* optical band for H α and [N II]. The profiles with the same colour are constrained to have the same FWHM and shifts. The magenta curves are the sum of the different components. The blue and green lines represent the two Gaussian components of the broad emission lines of Ly α , N V and C IV. The red lines are the narrow components used to calculate the narrow-line ratios, e.g. [O III]/H β and [N II]/H α . The light blue lines are the wing components of [O III] $\lambda\lambda$ 4959, 5007. The brown and cyan lines are the broad components of H α and H β . The light green and yellow lines are the third components in seven objects whose broad lines of H α and H β clearly have different shapes. See the text for details on the fitting procedure (§2.3). Residuals are obtained by subtracting the sum of all the components from the spectra, and the unit is $10^{-15} \text{ erg s}^{-1} \text{ cm}^{-2} \text{ \AA}^{-1}$.

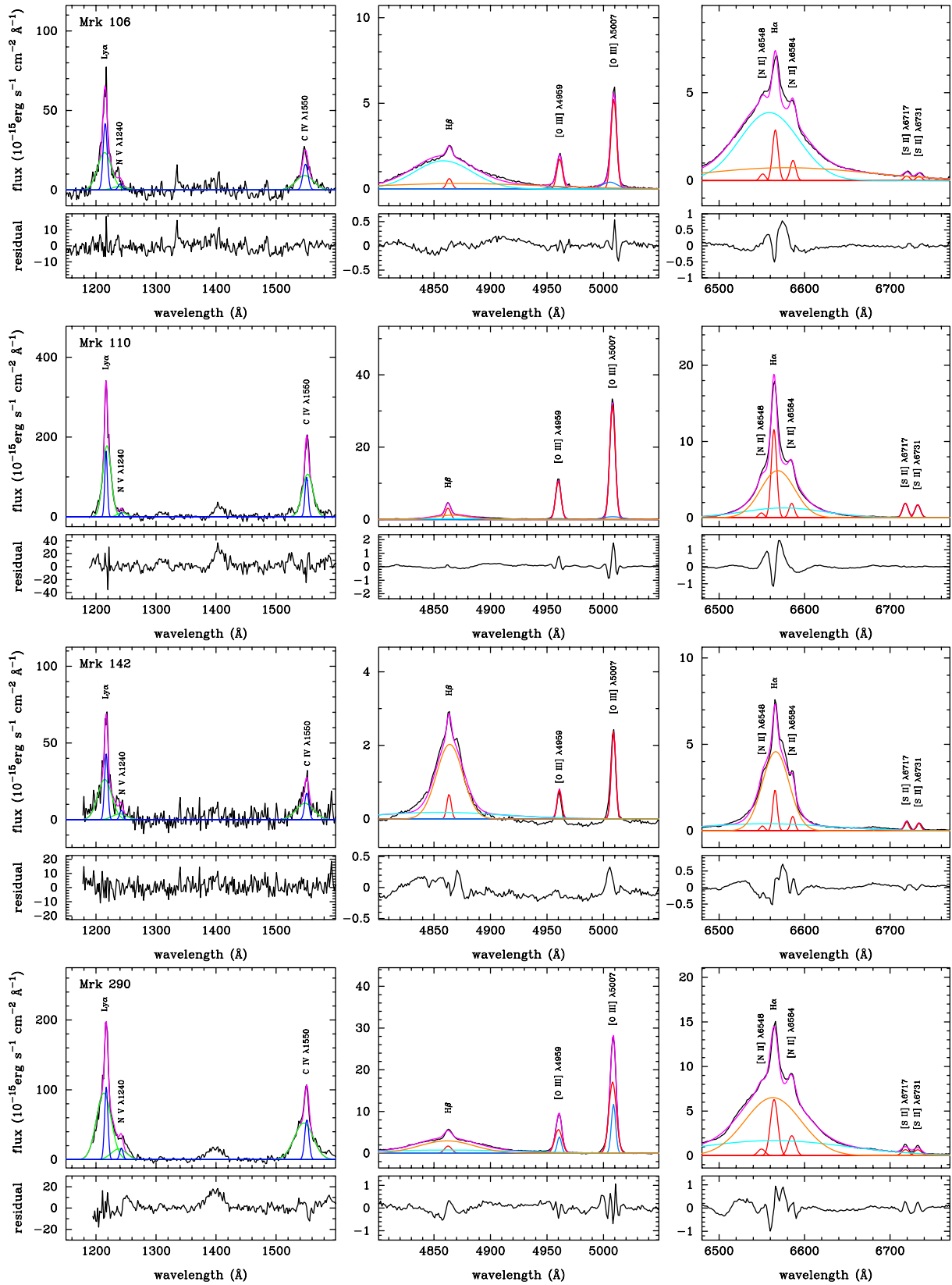


Figure A2. Fig. A1 continued.

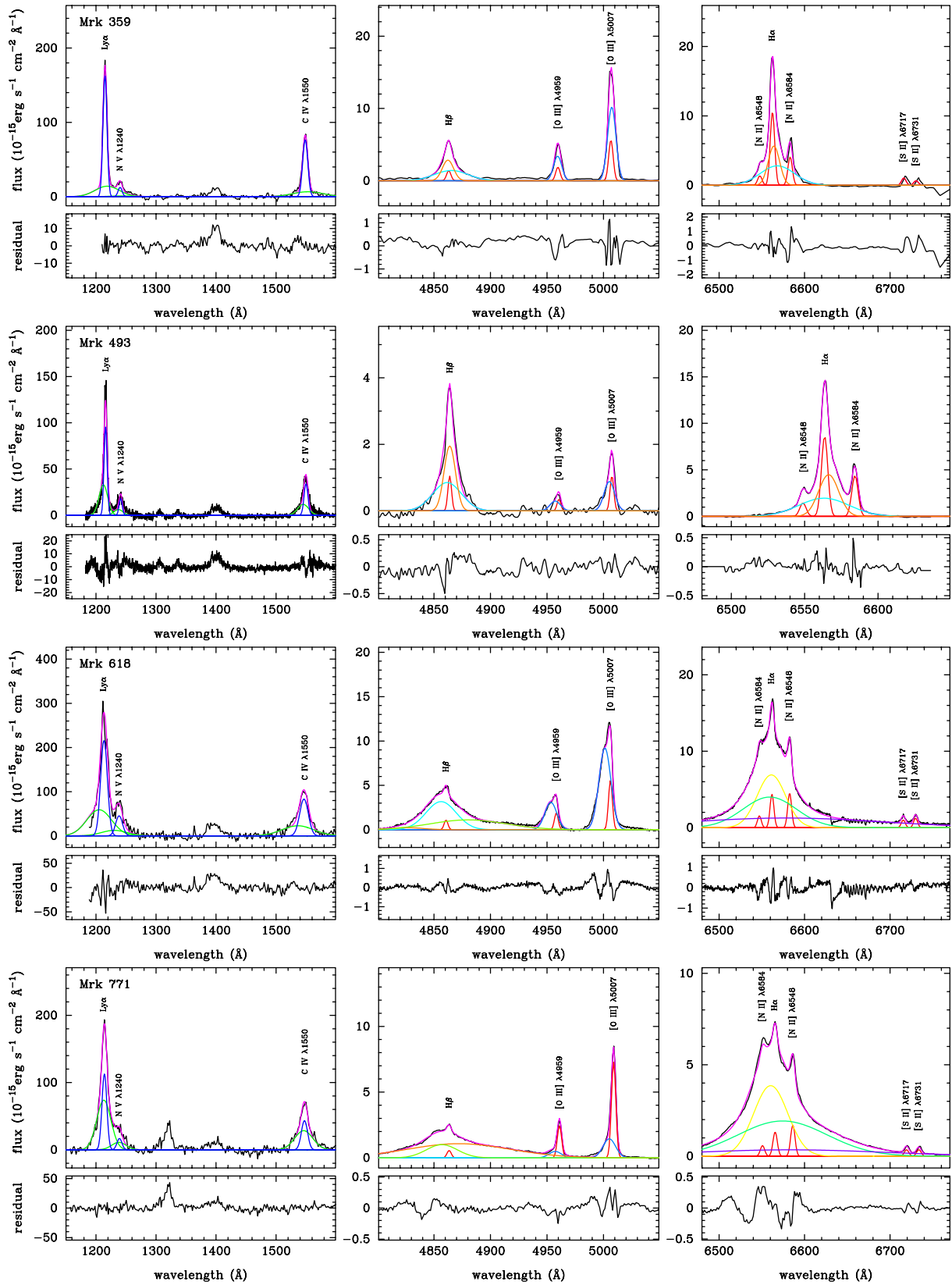


Figure A3. Fig. A1 continued.

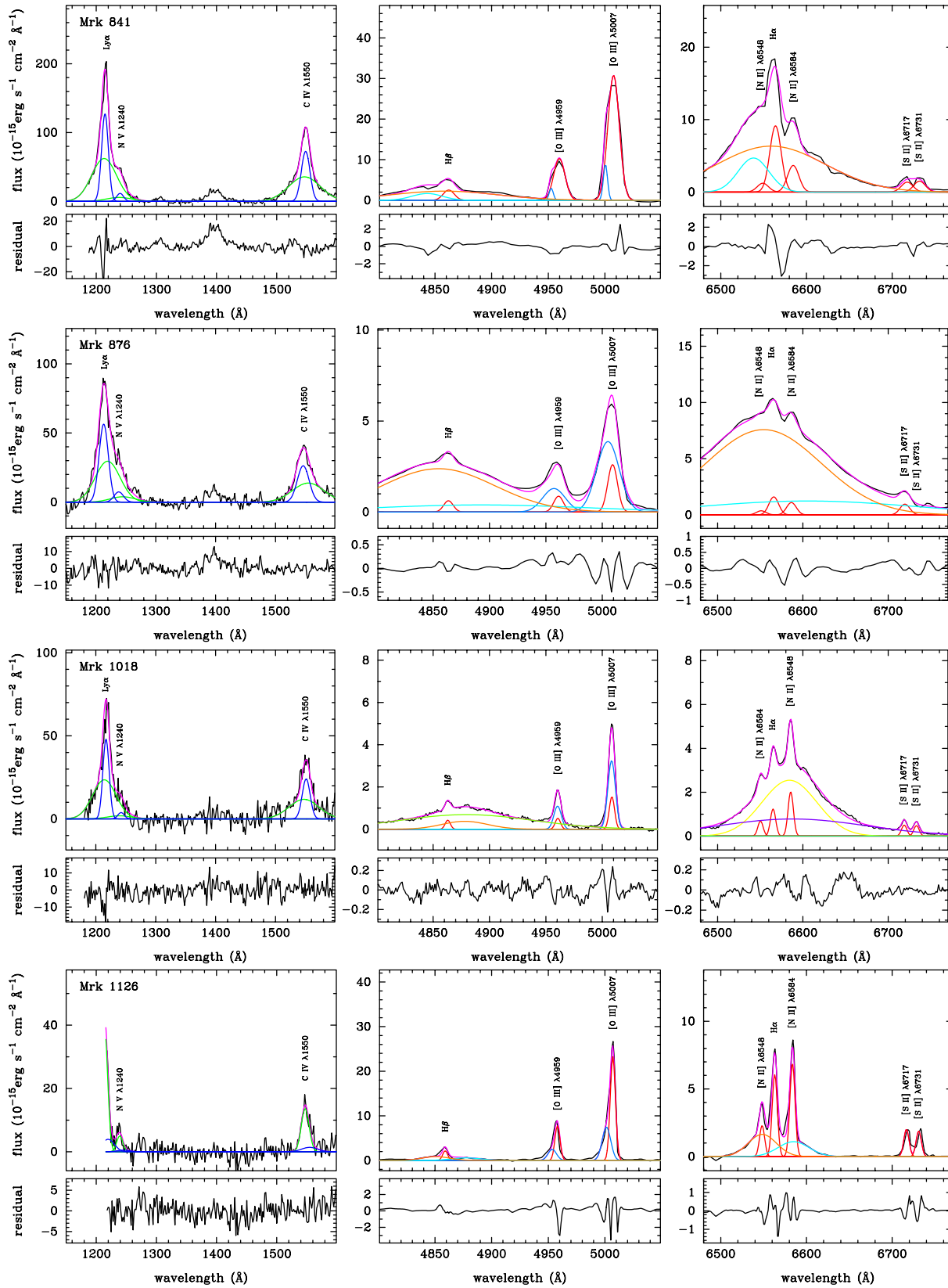


Figure A4. Fig. A1 continued.

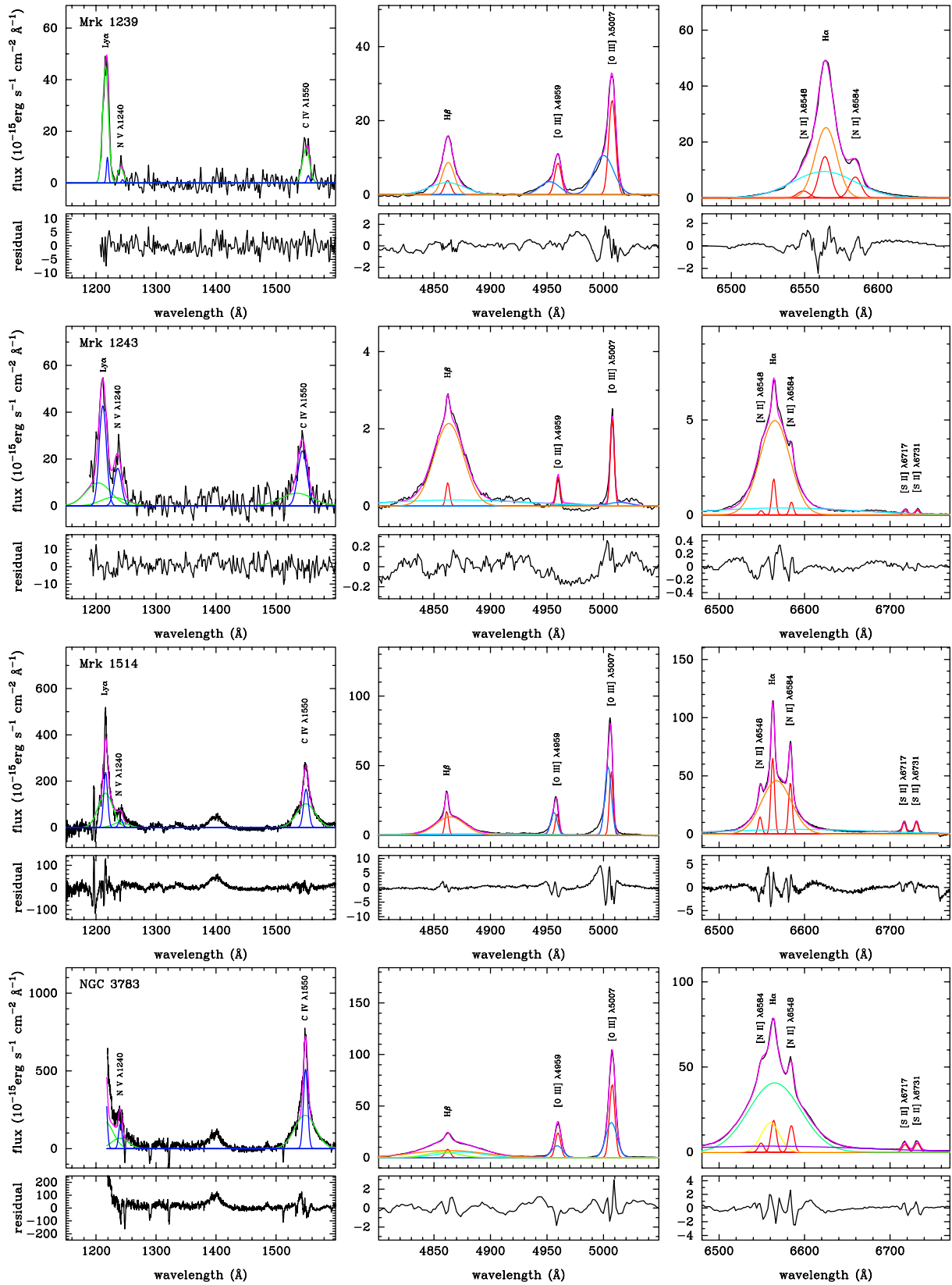


Figure A5. Fig. A1 continued.

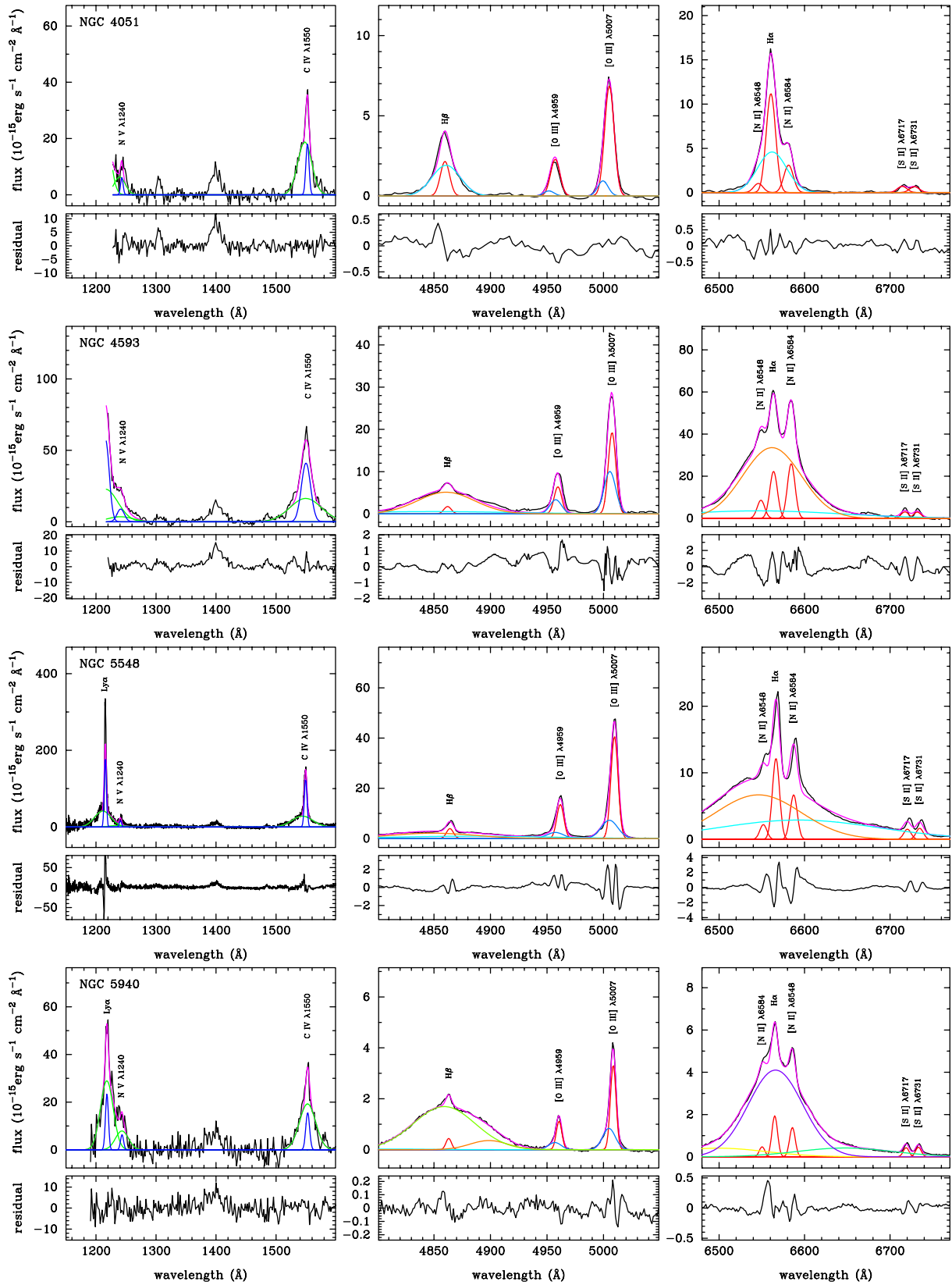


Figure A6. Fig. A1 continued.

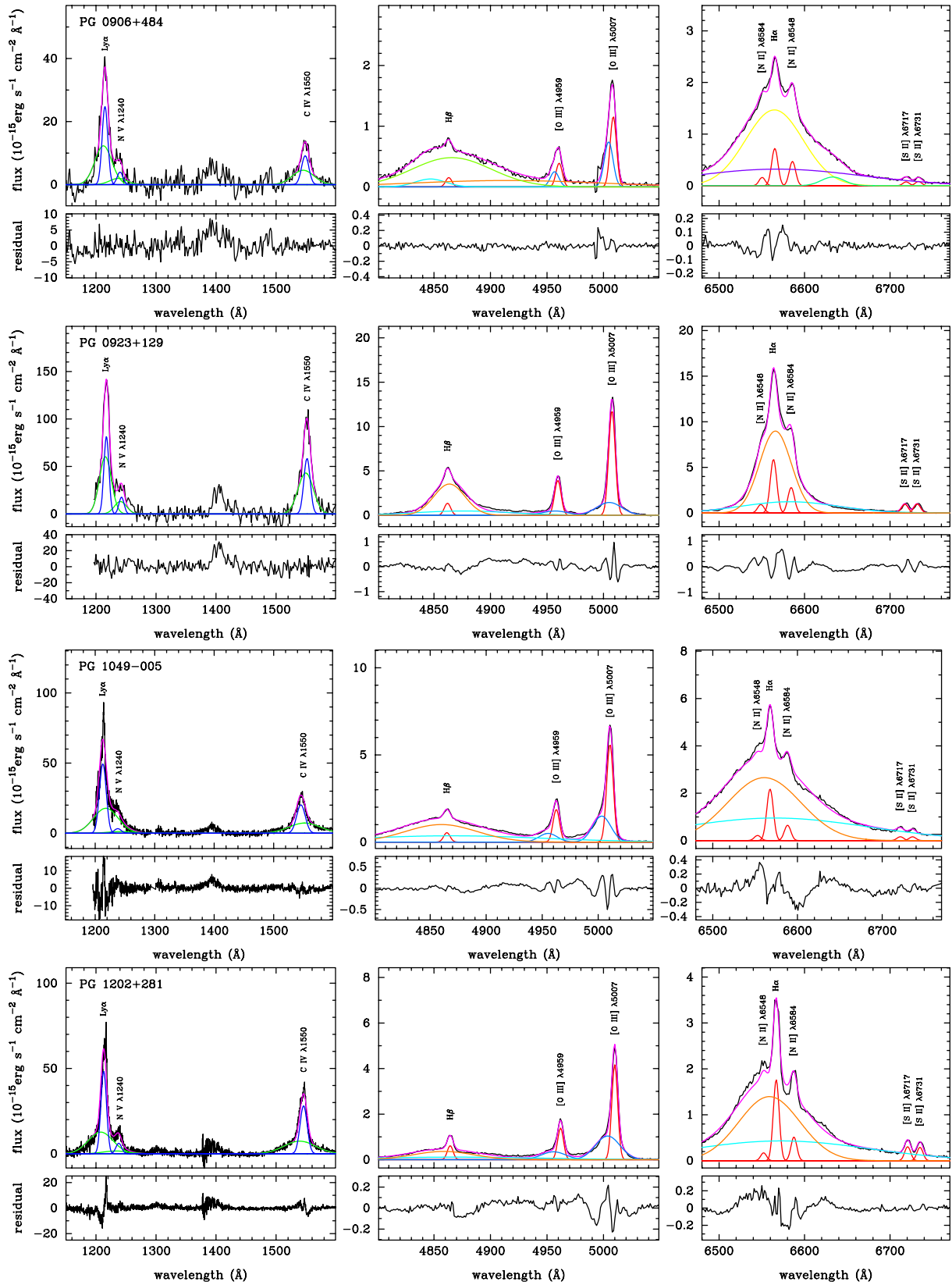


Figure A7. Fig. A1 continued.

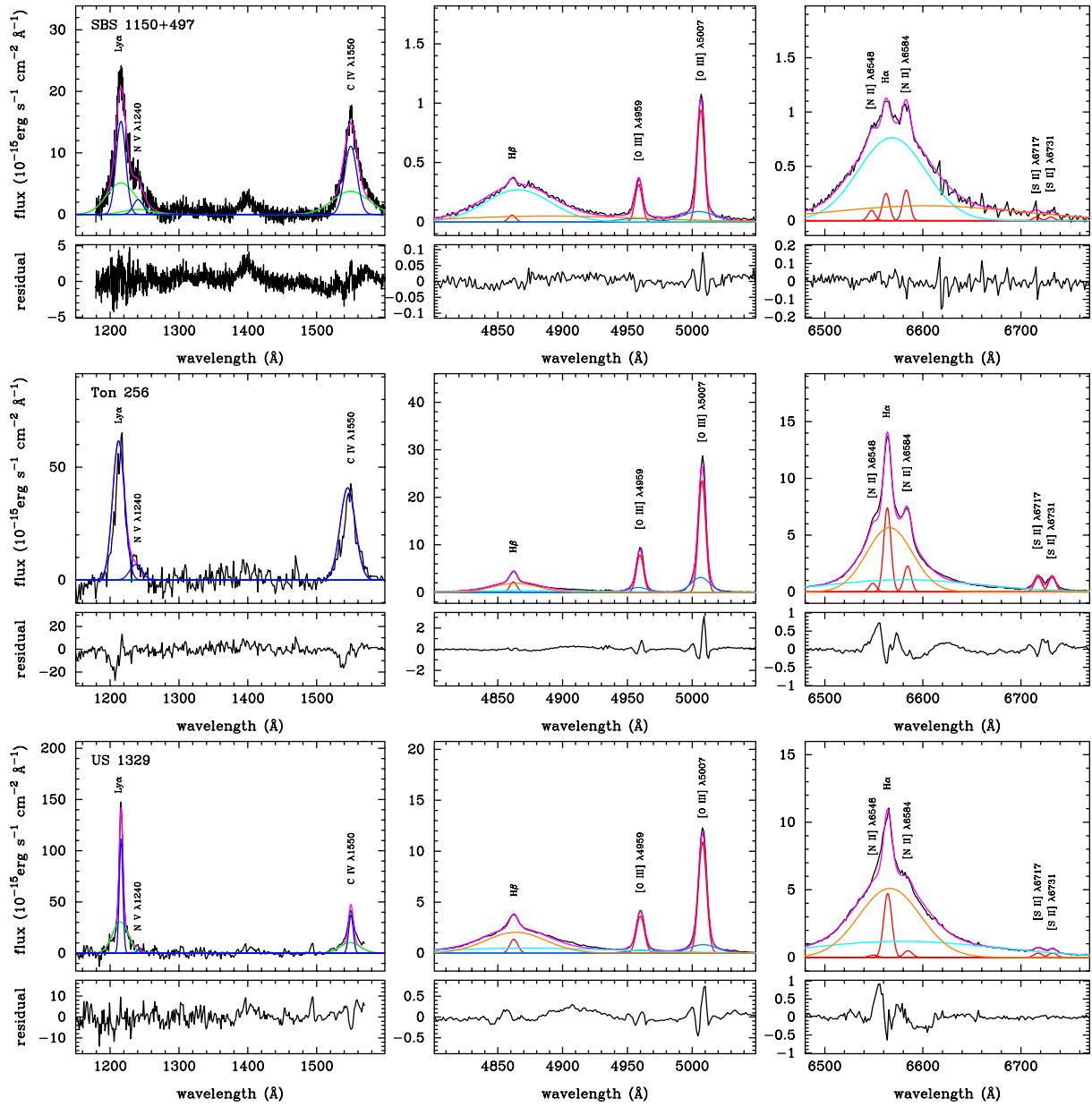


Figure A8. Fig. A1 continued.